J Ther Eng, Vol. 11, No. 5, pp. 1293−1311, September, 2025

Journal of Thermal Engineering
Web page info: https://jten.yildiz.edu.tr
DOI: 10.14744/thermal.0000976

Research Article

On the role of biomimetics shark skin flow control in the aerodynamic characteristics of leading-edge protuberanced wing section

S. SMRITHIKA[1], S. ARUNVINTHAN[1,*]

[1]*Department of Aerospace Engineering, SASTRA Deemed University, Thanjavur, Tamil Nadu, 600001, India*

ARTICLE INFO

Article history
Received: 28 May 2017
Accepted: 08 August 2017

Keywords:
Aerodynamic Force Coefficients; Biomimetics; Flow Control; Leading-Edge Protuberances; Surface Pressure Distribution; Time-Series Data; Wind Tunnel Testing

ABSTRACT

An experimental investigation of the effect of shark skin flow control structures on the aerodynamic characteristics of novel bio-inspired Leading-Edge Protuberanced wing section is presented in this paper. NACA 63(4)-021 airfoil based leading-edge protuberanced wing featuring an Amplitude of 0.12c and wavelength 0.5c is utilized in this study. Short-fin Mako's scale structure as outlined in the previous literature were 3D Printed and they act as the base geometry of the shark scale structure. Two different sets of shark scale geometries, varying in chord length, span, amplitude, and wavelength were chosen based on the literature. Additionally, to assess the significance of the alignment of these 3D Printed shark scale structures on the aerodynamic characteristics, different patterns like Staggered non-overlapped, linear non-overlapped, linear overlapped were considered. This study merges two biomimetic ideas such as leading-edge protuberances and shark scales which renders aerodynamic benefits. The focus of this study is to assess the influence of the shark scale structures as an effective flow control means for biomimetic Leading-Edge Protuberanced Wing section. Further, all the works related to shark scale were only carried out over conventional straight wing airfoil sections. The present study is the first of its kind to investigate the influence of shark scale structures on the aerodynamic characteristics of Leading-Edge Protuberanced wings. All the series of experiments were conducted at wide range of angles of attack ranging from $0° \leq \alpha \leq 70°$ in an increment of 5° at two different Reynolds number 32066 and 69488. Surface pressure measurements were obtained over the test models with the help of Miniature Pressure Scanner 4264 Scanivalve pressure scanner pneumatically connected to the 50 pressure taps equi-distributed over the upper and the lower surface of the test model. Results reveal that the use of shark scale structures as a means of flow control renders aerodynamic benefit in terms of lift increment, drag reduction and stall delay. The modified LEP model with Shark scale structures exhibit 34.6% increment in lift coefficient, 29% decrement in drag coefficient and 42.8% stall delay. The modified shark scale model fitted Leading-Edge Protuberanced wing is effective and outperforms conventional Leading-Edge Protuberanced wing especially at low Reynolds number and hence could be used as a viable solution for Micro-Aerial Vehicles and Nano-Aerial Vehicles operating in this regime.

Cite this article as: Smrithika S, Arunvinthan S. On the role of biomimetics shark skin flow control in the aerodynamic characteristics of leading-edge protuberanced wing section. J Ther Eng 2025;11(5):1293−1311.

***Corresponding author.**
*E-mail address: smrithika613@gmail.com, sarunvinthan@gmail.com

This paper was recommended for publication in revised form by Regional Editor Ahmed Selim Dalkilic

INTRODUCTION

Airfoils invention dates back to 19th century and over the years it has become omnipresent. Airfoils have now emerged as a crucial component of several man-made Engineering structures like propellers, marine rudders, wind turbine blades, high-lift devices of airplanes, control surfaces of missiles etc., as illustrated in Fig. 1. Despite the application field, it remains common that the flow over the airfoil must remain attached to the surface as long as possible even at greater angles of attack for increased performance in the airfoil. Flow separation is one of the major issues which plagues the aerodynamic performance of the airfoils|. To mitigate this risk and reduce its influence, Flow control techniques have emerged and several researchers and engineers adopted several flow control strategies over the years. Therefore, it becomes clear that the flow control technology has emerged as a promising solution to conquer the terrible aerodynamic performance triggered by the boundary layer separation on airfoil's suction surface as airfoils are ubiquitous [1]. The flow separation over the airfoils can be controlled by three methodologies namely active, passive and hybrid. As we know that the when both the active and passive flow control techniques are incorporated together, they give rise to a hybrid flow control technique. Based on the literature, it is evident that the passive flow control techniques are popular as they require minimum energy intervention as they don't require any active energy source.In addition, because of its intrinsic simplicity accompanied with economy, it is one of the most viable solutions as a flow control means. Recently, researchers have started focusing their attention on optimizing the Unmanned Aerial Vehicles (UAV), Micro-Aerial Vehicles (MAV) and Nano-Aerial Vehicles (NAV). Micro Aerial Vehicles and Nano Aerial Vehicles are recently utilized as the First-Person View Drones in the real-world combat scenarios. Due to its small size and operating Reynolds number (Re), without an effective flow control method, the MAV/NAVs face aerodynamic challenges which can lead to unstable and unpredictable airflow. An effective flow control means like shark scale structures will help stabilize the airflow around the vehicle, improving overall stability and control thus rendering more accurate control of lift, drag and other aerodynamic forces. In this way, it can reduce the power required for the flight, thus increasing the endurance i.e. Extended flight time / Range translating to longer flight times. FPV operating in closed building will experience turbulence mitigation and increased agility allowing for quick response to changes in the environment which is vital. As flow control effectively reduces the acoustics signature, it can also lead to quieter operation. Given the prevalence of airfoils in aircraft, UAVs, MAVs, and NAVs, wings, control surfaces etc., it is thought to be essential to predict their aerodynamic performance under various wind characteristics to withstand and lessen the adverse consequences.

With the advancements in the technology, biomimetics can be considered as an option to effectively control the flow over the airfoils. One such intellectual way is to have a look into shark's denticular shape as a form of passive vortex generator over the airfoil. Shark skin has dermal denticles (scales) that impede body separation by providing local flow separation control, thus helping the shark to swim faster in water with least drag. The shark scale is replicated as vortex generator in the previous research of Arunvinthan et al. [2]. Based on the results reported by Arunvinthan et al. [2], the use of Shark scale-based vortex generators (SSVGs) has improved the coefficient of lift by 3.8%, contributing to

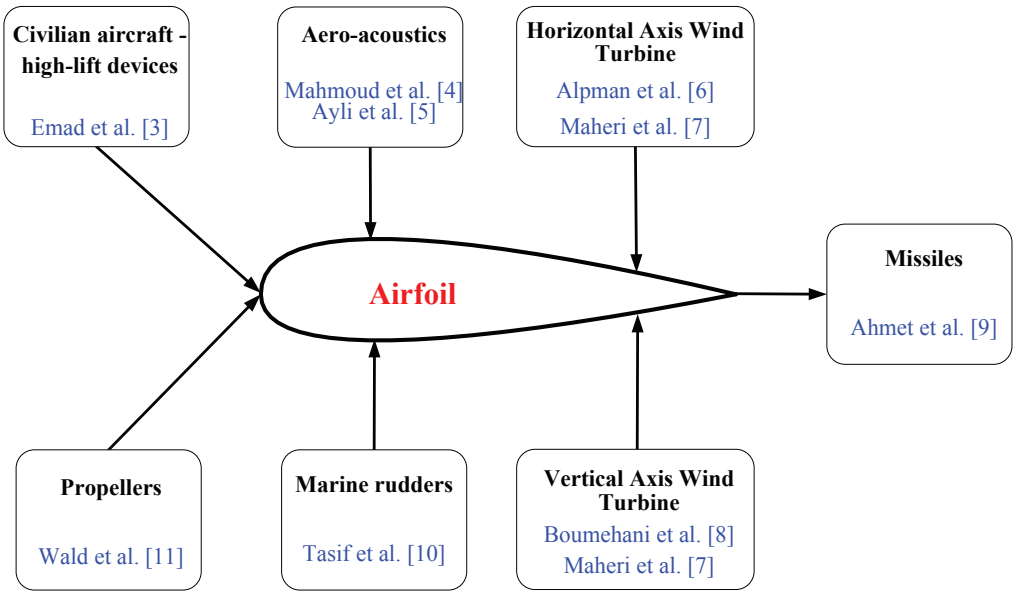

Figure 1. Few applications of airfoil [Created by authors].

drag reduction and delays the stall by regulating the flow separation. It was discovered that bristled denticles on the shark skin act as a vortex generator which is a passive flow control mechanism.

Lang et al. [12] investigated the microgeometry of the shark scale and reported that the cavity like structure formed over the denticles plays a vital role in suppressing the wake formation. Lang et al. [12] investigated the complex 3d embedded cavity model and compared its result with the flat base (i.e. square cavity) model and revealed that the shark skin structure forms a series of interlocking web of vorticity thus promoting drag reduction. Bechert et al. [13] claimed that the shark scale structures behave in a similar way as riblets based on the SEM analysis. Bechert et al. further continued his research [13] by replicating 800 plastic scales with compliant anchoring over a flat plate resembling shark scales and tested whether they can be used as a viable alternative for vortex generators to suppress the flow separation. From the results, it has been identified that the vortices created along their axis in the streamwise direction by shark scales induces momentum in to the flow and promotes exchange of momentum thus leading to an increased flow velocity near the wall. Motta et al. [14], identified that the shark skin denticles are composed of tooth-like layers of enameloid and dentine with a central pulp cavity, and have an expanded base that anchors individual denticles into the skin as shown in Fig. 2. Utilizing similar morphology as found by Motta et al. [14], Li Wen et al. [15] designed and manufactured flexible biomimetic shark skin models using 3D Printing. Li Wen et al. [15] focused his attention on the effect of shark scale pattern over the flat plate in water tunnel. Aiming at identifying the influence of the patterns on the drag characteristics, three different alignment patterns were utilized. Based on the research findings, Li Wen et al. [15] reported that the staggered–overlapped pattern offers exceptional swimming speed with reduced drag at low speeds when compared against the other 2 alignment patterns. This clearly shows that the pattern of shark scale also plays an important role in determining the drag characteristics. However, to quantify that, Bechert et al. [13], established a numerical relation using a dimensionless parameter S+ to represent the effective Re based on the spacing between the denticle top ridges. S+ can be mathematically represented as shown in Eqn. (1) where, S is the spacing between the adjacent denticle ridges, ρ the fluid density, υ the kinematic viscosity and τ_w being the average shear stress.

$$S^+ = \frac{S}{\upsilon}\sqrt{\frac{\tau_W}{\rho}} \tag{1}$$

The spacing between the adjacent denticle ridges (s) can be seen from the zoomed-in view of the sagittal section as shown in the Fig. 2. With the advent of latest digital manufacturing techniques, researchers adopted the methodology of 3D printing shark scale structures to mimic them and obtain the aerodynamic benefit over airfoils. Some of the recent literatures like Arunvinthan et al. [2], Li wen et al. [15-16], Yuji Yasuda et al. [17], Wen Chien et al. [18] etc., has utilized 3D printed shark scales in their research. Li wen et al. [15-16] have mimicked the real-time shark scale and 3D printed them to experimentally investigate the hydrodynamic characteristics of the shark skin membrane. The shark scales were scaled up around 12.4 times due to the technical limitations involving degradation of shark scale denticles when printed at real-time shark scale dimensions are associated with 3D printing technology. Yuji Yasuda et al. [17] mentions about the challenges in manufacturing due to scaling and cost. Furthermore, Wen Chien et al. [18] indicated that the shark scale structures manufactured using 3D printing lack surface hydrophobicity and could potentially create biological settlement. To overcome which, their report suggested anti fouling coating using enzymes (which includes a combined chemical effect) which makes the 3D Printing a lot difficult when we make it in microscopic level. Despite several researchers focusing their attention on such 3D Printed

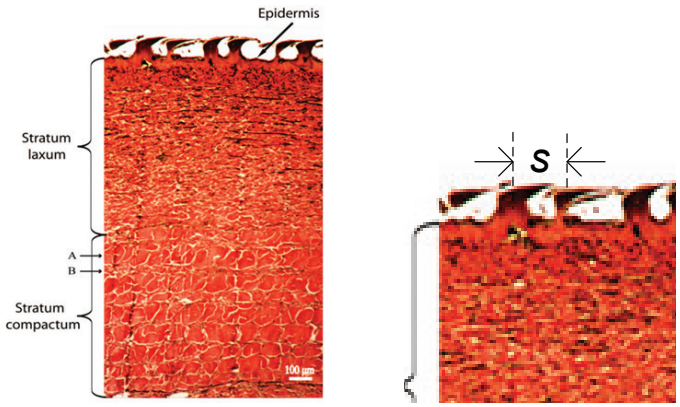

Figure 2. Sagittal section through the skin of a female shortfin mako shark Isurus oxyrinchus and its zoomed-in view [Bechert et al. [14], with permission from John Wiley].

shark scale structures, it is worth noting that the least sizing which a 3D printer can print is of no match to the actual real-world shark scale which is one of the primary challenges involved. Another challenge involved in designing and manufacturing the shark scale is because of its complicated design geometry. Domel et al. [19] morphologically investigated the shark skin and identified that shark skin is covered with rigid bony denticles that with ridges which narrows to a thin neck that anchors into the skin and contribute to drag reduction effect and claims that the shark scales play a significant role in the lift enhancement providing high lift to drag ratio. Their research results revealed that the boundary layer formed near the shark scale helps in generating a short separation bubble which in turn creates a low-pressure region (i.e., suction) over the upper surface of the airfoil causing the flow to reattach thus improvising the lift and rendering aerodynamic benefits. In addition, the streamwise vortices generated by the shark scales or denticles prevent loss of lift at high angles of attack and increment in drag. Similarly, C. Lee et al. [20] numerically investigated about the rectangular sharklet patterned membrane under two flow conditions which confirmed that the sharklet pattern is favourable in flow re-attachment. Following which Fagla J. Mawignon et al. [21] investigated riblets orientation and the arrangement patterns to optimize the results. To characterize the alignment of the riblets in both the laminar and turbulent flow two patterns namely aligned and staggered pattern were evaluated. The investigation reveals that aligned and staggered arrangements of the simplified shark scale structures reduce the drag effectively about 11.3% in laminar state and 6% in turbulent state. From the results, it becomes clear that the shark scale structure effectively alters the flow characteristics based on their sizing and alignment pattern. Shuai Li et al. [22] also investigated the drag reduction mechanism of bionic skin made of scale structures and reported that the bionic skin generates vortex structure which favours the drag reduction by flow re-attachment. However, to identify any influence of the rigidity of the scale, Dengke Chen et al. [23-25] have experimentally investigated the effect of bionic gradient flexible fish skin on the drag characteristics and revealed that it also reduces the drag effectively. Furthermore, D. Chen et al. [23-25] carried forward the research to evaluate the effect of multi-scale and multi-level riblet on the drag characteristics by considering various fish skin like shark skin, dolphin skin, tuna skin etc. The multi-scale and multi-level riblet which was inspired from the shark skin has been fabricated and the results conclude that multi-scale and multi-level riblet surface provides a maximum drag reduction ratio of 6.35% at the Reynolds number in the order of 10^5. Dengke Chen et al. [23-25] also has identified and reported intricacies like fabrication of shark skin due to the complex topography of the shark skin in their literature. Recent literatures claim that the

Table 1. Literature review and its relation with the experimental findings

Author	Experimental / Numerical	Description	Characteristics	Relation with the findings
Bechert et al. [13]	Experiment	Vortices by the shark scales infuse momentum in to the flow resulting in drag reduction.	Hydrodynamics	Drag reduction
Lang et al. [12]	Experiment	Shark scale structures promote drag reduction by suppressing the wake formation.	Hydrodynamics	Drag reduction
Li Wen et al. [15-16]	Experiment	staggered-overlapped pattern offers high speed with reduced drag.	Hydrodynamics	Drag reduction
Domel et al. [19]	Experiment	Shark scale generates separation bubble causing the flow to reattach, thus improvising the lift coefficient	Aerodynamics	Lift increment
Arunvinthan et al. [2]	Experiment	SSVGs improved lift coefficient by 3.8%, contributes to drag reduction and stall delay	Aerodynamics	Lift increment, drag reduction and stall delay
Lee et al. [20]	Numerical	Sharklet patterns promote flow-reattachment	Hydrodynamics	Extended flow attachment
Mawignon et al. [21]	Numerical	Staggered outperforms the aligned pattern of riblet surface.	Hydrodynamics	Drag reduction.
Shuai Li et al. [22]	Numerical	Delays the flow separation and reduces drag.	Hydrodynamics	Extended flow attachment and Drag reduction.
Dengke Chen et al. [23-25]	Experiment	Multi-level riblets provide maximum drag reduction ratio	Hydrodynamics	Drag reduction.

shark-skin inspired thin film attached to the airplane exhibits a reduced drag and reduction in fuel consumption which necessitates the study to be developed further in the domain of space and aviation.

It The present study aims at investigating the effectiveness of shark scale structures as an flow control method over airfoils by experimentally evaluating two different shark scale structures under three different alignment patterns for a wide range of angle of attack ranging from $0° \leq \alpha \leq 70°$ in an increment of 5° at two different Re = 32066 and 69488. This will act as a pilot study for administering shark scale structures as an effective flow control method for airfoils. Most of the previous literature explores the feasibility of shark scale structures as an effective means of drag reduction methodology to augment the hydrodynamic characteristics. Even though the use of shark scale in hydrodynamics has a strong foundation, limited number of studies were conducted in aerodynamics. To the extent of author(s) knowledge, the knowledge of shark scale structures on the aerodynamic characteristics remains unclear, and is yet to be explored. It is worth noting that this domain is less explored because of the challenges associated with the manufacturing (3D printing) of complicated shark-scale geometries, fixing them over aerofoils and in obtaining real-world Reynolds number scenarios. Further, all the works related to shark scale were only carried out over conventional straight wing airfoil sections. The present study is the first of its kind to investigate the influence of shark scale structures on the aerodynamic characteristics of Leading-Edge Protuberanced wings (inspired from the flippers of the Humpback whales featuring varying chord along the span). Additionally, the present study acts as a bridge between two successful biological inspirations from nature. Therefore, the present study will help aerodynamic designers in identifying the optimum denticle pattern, size and shaping at low Reynolds number for the possible application over UAV/MAV and NAV with immediate effect. Table 1 represents the relation between the literature and experimental findings of the present study.

EXPERIMENTAL METHODOLOGY

The effect of shark-scale structure and its alignment on the aerodynamic characteristics of NACA 63(4)-021 airfoil based biomimetic leading-edge Protuberanced wing was experimentally evaluated in this paper at Re=32066 and 69488.

Wind tunnel: All the experimental evaluations carried out in this study were conducted at a low-speed subsonic wind tunnel facility located at SASTRA Deemed University. This wind tunnel encompasses a rectangular test section with cross section of 300x300x1500 mm. The tunnel is operated by a fan powered by a 10HP motor and may attain a maximum wind speed of around 60 m/s. The free stream turbulence intensity is 0.51%. A schematic representation of wind tunnel facility with necessary equipment set up is shown in Fig. 3 and the real images of Low-speed subsonic wind tunnel facility is shown in the Fig. 4.

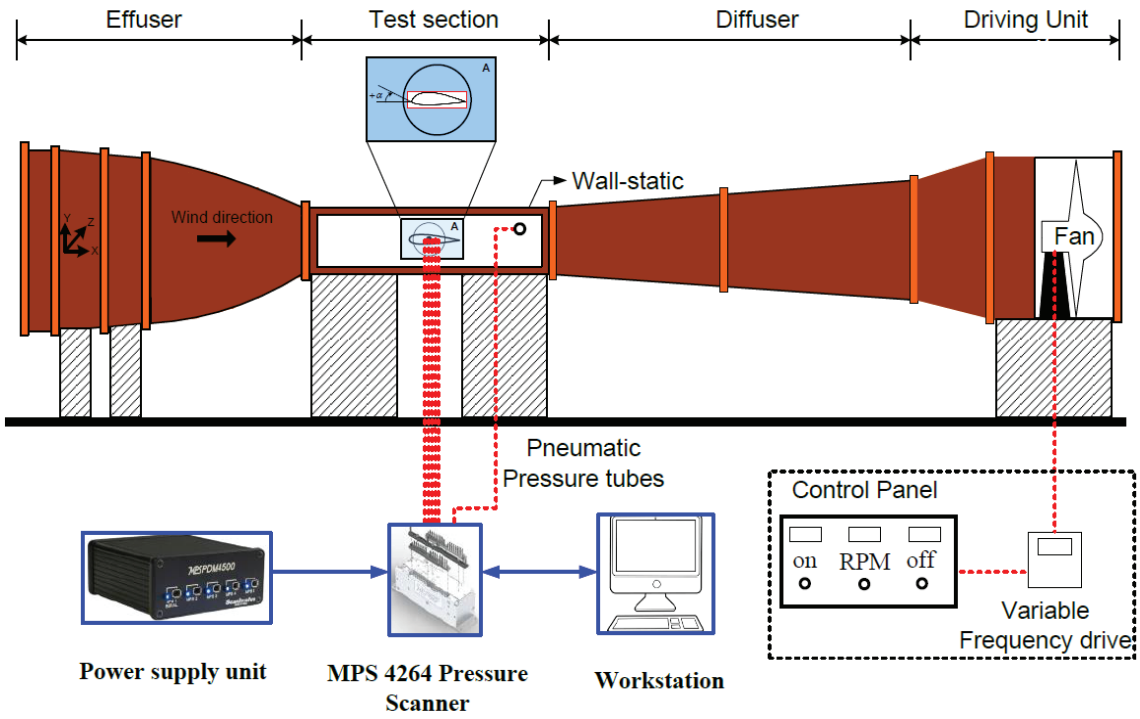

Figure 3. Wind tunnel facility equipped with MPS 4264 Scanivalve pressure scanner.

Figure 3. Low-speed subsonic wind tunnel facility

Table 1
Geometrical parameter of the test model.

A/c	λ/c	Label
1	1	Baseline
0.025	0.5	Small LEP
0.1	0.25	Medium LEP
0.12	0.5	High LEP

Test model: NACA 63(4)-021 airfoil model was chosen as the base model as it closely resembles the cross section of the humpback whale flipper which acts as a bio-inspiration for the LEP wing. Since the present study aims at investigating the effect of shark-scale surface and its alignment pattern on the aerodynamic characteristics of NACA 63(4)-021 airfoil based biomimetic leading-edge Protuberanced wing, the baseline model is a LEP Wing. Based on the framework of the previous researchers [26], it becomes clear that the LEP wing features a sinusoidal leading-edge profile influenced by two geometrical parameters named Amplitude (A) and wavelength (λ). It should however be noted that as the present study focusses its attention on investigating the effect of shark scale surface and its alignment pattern alone, the amplitude and the wavelength of the LEP is kept constant throughout this paper.

Based on their experimental evaluation, it has been identified that the A=0.12c and λ=0.5c renders optimum aerodynamic benefit and outperforms the other two test cases. Therefore, the same A=0.12c and λ=0.5c has been chosen as the baseline model for this present study. The airfoil considered in this study is assumed to have a mean chord length of 100 mm and span 300 mm which signifies that the test model is an infinite one. The full-span model was then fabricated by 3d printing using polylactic acid (PLA) material at the resolution of 100 microns. There are special recommendations for distributing the surface pressure taps over the LEP airfoil. As the test model is a non-constant chord model, the surface pressure distribution needs to be measured at two different locations namely peak (chord maxima) and the trough (chord minima) which is one of the special requirements of the LEP wing. A total of 50 pressure tapings were made over the surface of the model. 20 pressure taps were equi-distributed along the peak and 16 taps over the trough region while the remaining taps were distributed along the span. The diameter of each pressure tapping is approximately 1mm with the spacing between each pressure tapings as 9 mm [26]. The airfoil model considered in the present study is the same considered in the previous study by Arunvinthan et al. [26]. Henceforth, the results are validated against the previous research paper [26] as shown in the Fig. 5 and the results reveal that the validation holds in good agreement with the paper with a minimum error of 0.68% and maximum deviation of 12%. The difference in the values can be owing to the increase in the number of pressure ports on the present study from 36 to 50. Furthermore, since the present study is the pilot study in incorporating 3D Printed shark scales over the LEP airfoil, shark scale affixed structure cannot be validated. The dimensions of the test model and the schematics of the baseline LEP model and modified LEP model is represented in the Fig. 6 & 7.

Shark-Scale Surface: Based on the framework of the previous researchers, it has been reported that the morphometric measurements of shortfin mako scales were found to be of height height 0.03 mm, spacing ~ 0.04 - 0.08 mm, chord length of 0.169-0.214 mm, span length of 0.14 – 0.244 mm as digitized by Motta et al. [15].

As we know that the denticle shapes and size are highly dynamic and is often subjected to change based on the location of the shark scale on the body, type of the fish etc., it becomes important to assess the denticles of different shapes and sizes. However, as the present study tries to mimic the short fin mako, the denticle shape becomes constant. Therefore, in this study, 2 shark-scale test models featuring

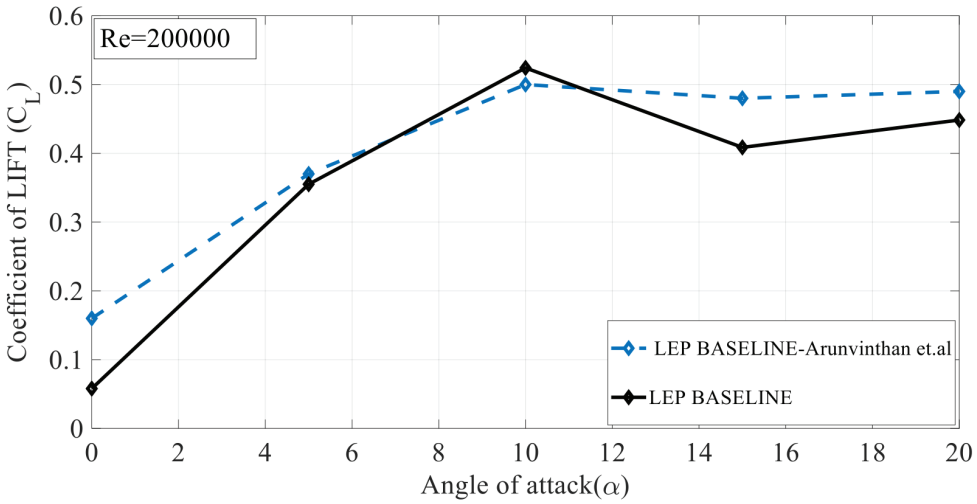

Figure 5. Validation of LEP baseline with previous literature.

Table 2. Geometric dimensions of 3D printed shark scales

Attributes	Small Shark Scale	Large Shark Scale
Chord length	10 mm	20 mm
Span	6 mm	12 mm
Leading-Edge Amplitude	2 mm	3 mm

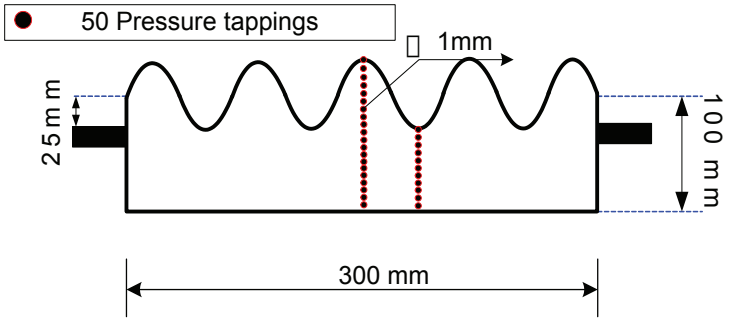

Figure 6. Dimensions of the test model.

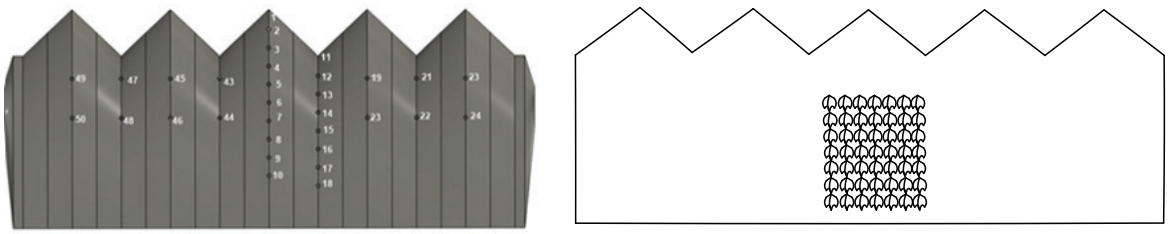

Figure 7. Schematics of baseline LEP model and modified LEP model.

chord length of 10 mm, span 6 mm with leading edge amplitude of 2mm (hereafter named as small shark scale) and the other model has a chord length of 20 mm, span 12 mm with leading edge amplitude of 3 mm (hereafter named as large shark scale) is considered. The geometric dimensions of the 3D printed shark scales are represented in the Table 2. One

could immediately note the difference in the size existing between the original morphometric measurements and the test model considered. This drastic difference in the sizing could possibly be explained by the limitations of the currently available 3D printers. In other words, due to the limitations in 3D printing resolution, the model was scaled up to the above stated dimensions. Yuji Yasuda et al. [17], Wen Chien et al. [18] etc. confirmed this limitation of sizing in using 3D printing in their corresponding research papers. In addition to this limitation, Yoseph Bar-Cohen et al. [27] emphasizes that nature's designs are optimized for specific environments and conditions that may not match the needs

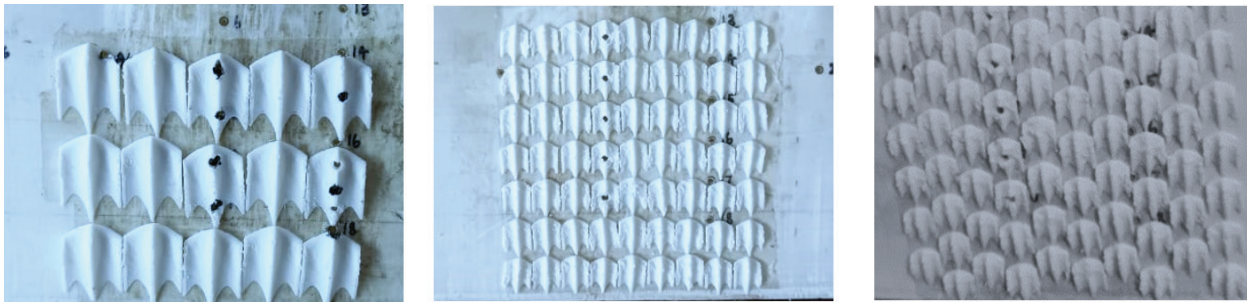

(a) (b) (c)

Figure 8. (a) large shark scale structure arranged in linear non-overlapped pattern (b) small shark scale structure arranged in linear overlapped pattern (c) small shark scale arranged in staggered non-overlapped pattern.

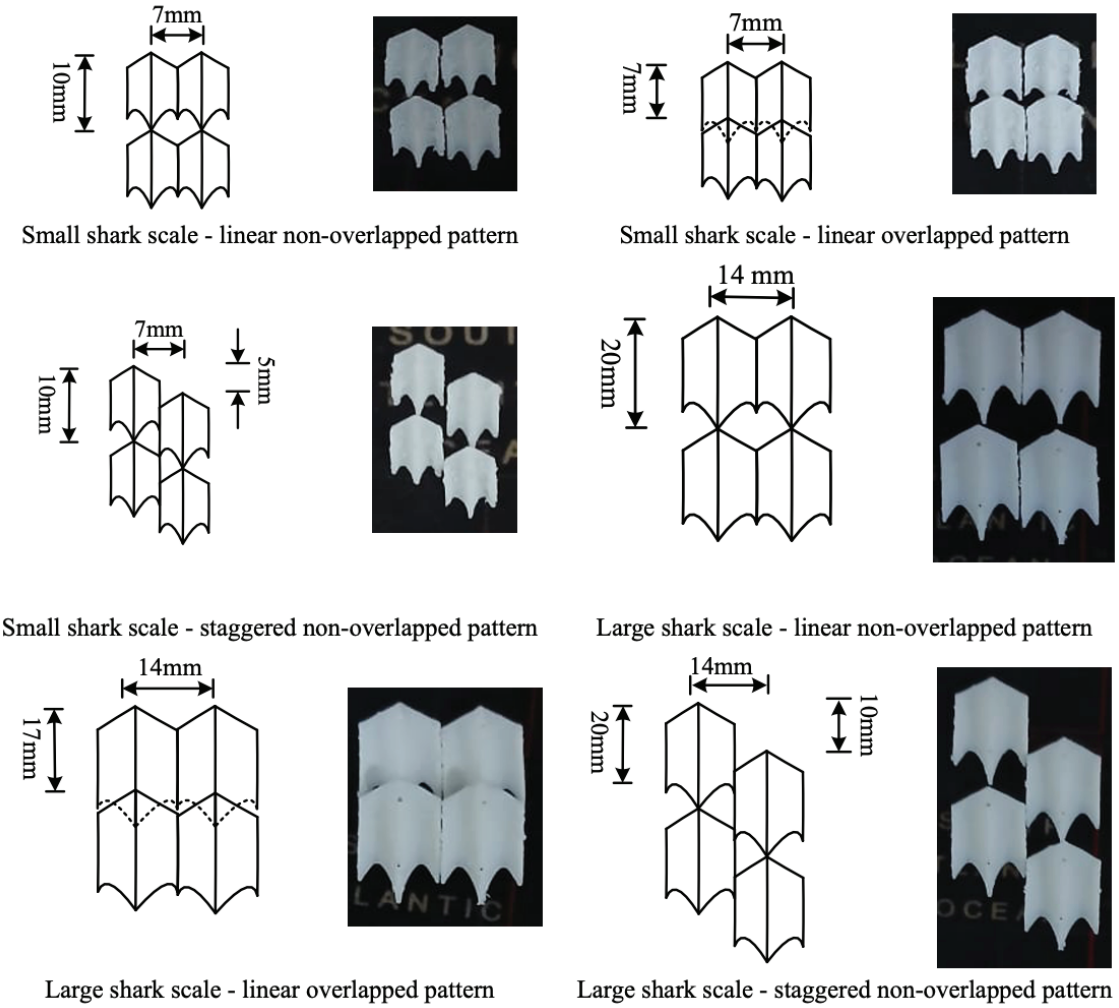

Figure 9. Schematics of alignment patterns for both large and shark scales.

of human applications. However, by making modifications and adapting these natural designs, it is possible to achieve functional and efficient solutions for technological challenges. This concept is central to biomimetics, where engineers and scientists take inspiration from nature's designs but modify them to fit specific human needs or constraints. Further, Li wen et al. [15] reported that although there is a great variety of denticle shapes and size, its intricate flow mechanism greatly depends on its complex patterns of alignment. To assess the significance of such complex alignment pattern in addition to the denticle size, three different patterns namely Staggered non-overlapped, linear non-overlapped, linear overlapped were inspired from the previous studies. A schematic representation is shown in Fig. 8. In this study, shark scale structures of different sizing were 3D printed using PLA material at a resolution of 100 microns per mm with ultra-marble finish. The 3D printed shark scale structures of different sizes were then blended over the leading-edge protuberanced wing with the help of commercially available non-residue double sided tissue tape having a thickness of 60μ. Schematics of alignment patterns for both large and shark scales are shown in Fig. 9.

Simultaneous pressure scanner: The surface pressure of the model is measured through the pressure taps on the surface which is pneumatically connected to MPS4264 Scanivalve pressure scanner. It has a range of 10" of H_20 water column with ±0.06% Full-scale, long-term accuracy as per the calibration certificate provided by the original equipment manufacturer (OEM). The time-series data obtained from the Scanivalve pressure scanner were collected at a sampling frequency of 700Hz corresponding to 10000 data samples. The aerodynamic lift and drag force acting over the biomimetic LEP Wing with and without shark scale structures were then estimated using pressure integration technique [26, 28-31] to yield the coefficient of lift and coefficient of drag.

$$F_D = \sum (\Delta P) \times S_i \times cos(\propto + \frac{\pi}{180}\theta) \tag{2}$$

$$F_L = \sum (\Delta P) \times S_i \times sin(\propto + \frac{\pi}{180}\theta) \tag{3}$$

$$C_D = {}^{F_D}/_{0.5\rho v^2 s} \tag{4}$$

$$C_L = {}^{F_L}/_{0.5\rho v^2 s} \tag{5}$$

Generally, the uncertainties in the experiments are due to the dispersion of the data or by the measuring equipment and instruments involved. Uncertainties associated with the wind tunnel like Buoyancy, solid blockage, wake blockage etc. and the instrumental uncertainties are discussed as follows.

Buoyancy correction: It is well known fact that boundary layer thickens as the flow travels downstream towards the exit cone thereby reduction in jet area and thus, inducing static pressure variation without the presence of test models. This could give rise to additional drag force and hence a suitable correction needs to be implemented on the experimental data. Glauert's method of buoyancy correction was implemented in the present study. According to Glauert, the total drag increment due to the buoyancy for a two-dimensional infinite model is:

$$D_B = \frac{1}{2}\pi\lambda_2 t^2 P' \tag{6}$$

where λ_2 is the body shape factor, t is the body thickness and P' is the slope of longitudinal static pressure gradient curve. The value for λ_2 for NACA 63(4)-021 airfoil used in this study is 1.4 as outlined in Barlow et al. [32]. The drag due to buoyancy was estimated as 0.009693 for this paper.

Solid blockage correction: The test-section walls reduce the area through which air flows when compared to free-stream conditions. Therefore, the velocity of the air increases as it squeezes through the reduced area in the vicinity of the model. This blockage is a function of model thickness, model distribution and the model size. This paper utilizes Thom's method of solid blockage correction for two dimensional tunnels:

$$\varepsilon_{sb} = \frac{K_1(Model\ Volume)}{C^{3/2}} \tag{7}$$

where K_1 equals 0.74 for wing spanning the tunnel breadth and C is test-section area. The model volume can be approximated as follows:

$$Model\ Volume = 0.7 \times model\ thickness \times model\ chord \times model\ span \tag{8}$$

The model volume was estimated to be 0.441 and the blockage correction was estimated as 0.01208 for this paper.

Wake blockage correction: The two-dimensional wake blockage correction provided by Allen and Vincentti was utilized in this paper. The wake blockage correction factor for two-dimensional case is:

$$\Delta C_{d,wb} = \Lambda\sigma \tag{9}$$

where Λ is body shape factor equals 0.36 for NACA 63(4)-021 airfoil as stated in Barlow et al. [32]. σ can be estimated from the formula

$$\sigma = \left(\frac{\pi^2}{48}\right)\left(\frac{c}{h}\right)^2 \tag{10}$$

and estimated as 0.0616225. The overall wake blockage correction was estimated to be 0.0221841 which is already implemented in the present manuscript.

Table 3. Pressure scanner accuracy

Full scale ranges	Accuracy	Over pressure capability	Operating Temperature
1 psid	0.06%FS	15x	0° -70° C

Table 4. Experimental dimensions table

Component	Dimension(s)	Component	Dimension(s)
Test section Length	1500 mm	Space between pressure taps	9 mm
Test section Width	300mm	Angles of attack	0°-70°
Test section Height	300 mm	Small scale chord length	10 mm
Maximum wind speed	60 m/s	Small scale span	6 mm
Mean chord length	100 mm	Small scale leading-edge amplitude	2 mm
Large scale leading-edge amplitude	3 mm	Large scale chord length	20 mm
Pressure taps diameter	1 mm	Large scale span	12 mm
Span length	300 mm		

Instrument and Data Error: The MPS4264 miniature Scanivalve pressure scanner utilized in the pressure measurement was precise with a full-scale error of ±0.06%, the correction affected only the third decimal of the uncorrected value. The accuracy of the pressure scanner is shown in the Table 3. The time-series data acquired from the MPS4264 Scanivalve pressure scanner shows a stationary data which indicates that the outliers or extreme values which can disproportionately affect the mean are absent. Also, since the process is automated using MATLAB, mistakes made during manual data entry, such as typographical errors capable of skewing the data is eliminated. Use of Scanivalve proved mettle in terms of calibration errors and drift in values. In short, the author(s) strongly believe that the data errors are kept minimum.

The drag due to Buoyancy is estimated as 0.009693 using Glauert's method; Solid Blockage is 0.01208 based on Thom's rule; Wake blockage correction is estimated as 0.0221841 utilizing Allen & Vincentti correction factor; Full-scale error of Instrument is ±0.06% based on the OEM Manual; Tolerance of 3D printer is ±0.1 mm. The detailed insights of the uncertainty measurements have been elaborated in the previous study [31-32]. Dimensions of all the components utilized in this study has been tabulated as shown in Table 4.

RESULTS AND DISCUSSION

The shark scale model affixed over the baseline LEP model was primarily examined to identify the influence of size and patterns on the aerodynamic characteristics of the LEP Wing at two different Re=32066 and 69488 and the corresponding results were presented and discussed in this section. The results were compared against the baseline LEP model to gain more insight about the effect of size and pattern of the shark scale structures on the biomimetic LEP Wing.

a) Re=32066:

The coefficient of lift for the clean baseline LEP wing and the modified airfoils affixed with two different shark scale geometries (i.e., small, and large shark scale structure) organized in three distinct alignment patterns operating at Re = 32066 is shown in Fig. 10. It can be observed from the figure that the unmodified model as well as modified model affixed with shark scale structures does not follow the conventional lift characteristics curve. It is speculated that this might be plausible due to the Reynolds number regime which is not conventional as well. Generally, it is known from the previous literatures that the clean baseline LEP wing tends to exhibit two-step stall characteristics. However, on the contrary, the clean baseline LEP wing did not exhibit two-step stall characteristics and follows an unconventional trendline of lift characteristics curve. Since the Re is very low, it is believed that the flow does not possess enough energy to follow the curvature prevailing at the nose region of the airfoil itself at $\alpha=0^{o}$. Furthermore, with the further increase in the angles of attack making it more difficult for the flow to remain attached over the airfoil might give an insight for this unconventional lift characteristics curve. Despite producing relatively lower lift coefficients, the modified models affixed with shark scales produce higher lift when compared against the baseline LEP wing. Based on the results, it has been identified that the incorporation of shark scale structures on the airfoil tends to transition the flow in to the turbulent regime thereby energizing the flow resulting in better flow characteristics. For instance. the lift coefficient for the 3D Printed

small shark scale model with linear non-overlapped alignment pattern exhibits two-step stall characteristics with the primary stall occurring at α = 30° and secondary stall happening at α = 50°. The two step stall characteristics which is reported in the LEP wing prevails with the addition of the shark scale structure. This clearly shows that the addition of shark scale structures on the LEP airfoils tends to augment its lift characteristics at the Re considered in this study. Likewise, a similar trendline of C_L is also seen in the small shark scale model with linear overlapped alignment pattern with primary stall occurring at α=15° and secondary stall happening at α=50° having a maximum C_L of 0.22 at α=50°.

Aiming at identifying the influence of staggered pattern, the small shark scale structure with staggered non-overlapped alignment pattern were also experimentally evaluated and the results show that the primary stall occurs at α=10° and the secondary stall happening at α=40°. Following which, to gain some more insight on the small shark scale structures, further analysis were carried out. It has been observed from the results that the presence of small shark scale structures over the LEP test model irrespective of the alignment pattern energizes the flow over the airfoil. This helps the modified model with shark scale structures exhibit delay in stall characteristics. For instance, it can be observed that a stall delay of 10° could be seen for modified small shark scale structure affixed LEP model in staggered non-overlapped alignment pattern than the linear overlapped alignment pattern. Based on these results, it can be concluded that the usage of the shark scale surface on the airfoil renders aerodynamic benefit in terms of stall delay. At the same time, it is worth noting that an abnormal trendline of C_L is seen for the large scale arranged in staggered non-overlapped pattern. This pattern produces a maximum lift coefficient of 1.2 at α = 15°. Beyond which with the further increase in the angle of attack, the lift coefficient gradually decreases. The lift coefficient for large scale arranged in linear overlapped pattern performs poorer than its counterparts. It is speculated that when these large shark scale structures are linearly overlapped, the first set of shark scales are aligned with zero degree of incidence to the flow. However, with the subsequent overlapping, from the second line of shark scale structures to the last line of shark scale structures, they experience a significant alteration in the incidence angle owing to overlapping. Therefore, the vortices induced from the first line of scale can be easily disturbed and trapped by the second line of shark scale structures inclined at an angle. Studies suggests that it resembles the bristling angle of the shark scale with one difference that in a conventional fish they are non-overlapped, but in this case, it gets overlapped which results in the detrimental result. As the momentum is not fully imparted in to the flow and gets trapped inside the incidence angle of the subsequent shark scale structures the net pressure gradient reduces. This gives the negative lift coefficient in comparison against the lift increment provided by other models. To further ascertain this behavior, it can be observed that, when the alignment pattern is changed from linear overlapped to staggered non overlapped, the energized flow arising out of shark scale structures moves over the surface of the airfoil without much hindrance, thus enabling better aerodynamic performance showing peak lift coefficient. Based on the results, it has been decided to eliminate the discussions on the linear overlapped pattern in further section because of its adverse nature.

The effect of shark scale on the drag characteristics is shown in the fig. 11. It is worth noting that the mean coefficient of drag plotted here represents only the pressure drag which is obtained from the airfoil surface pressure measurement and does not involve skin friction drag. Further, it can be inferred from the figure that the drag coefficient increases gradually till stall angle. Following that, a rapid increase in the C_D can be seen. The high turbulent mixing

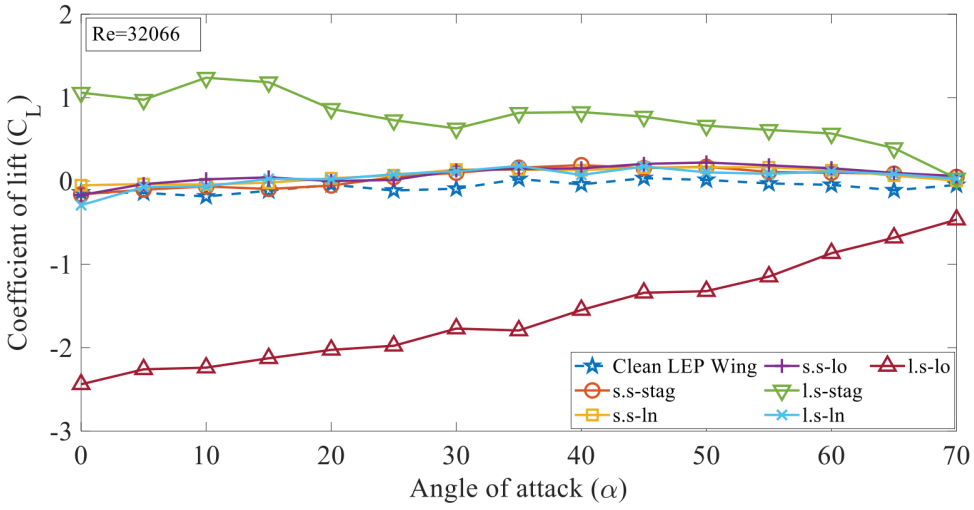

Figure 10. Coefficient of lift (C_L) vs Angle of attack (α).

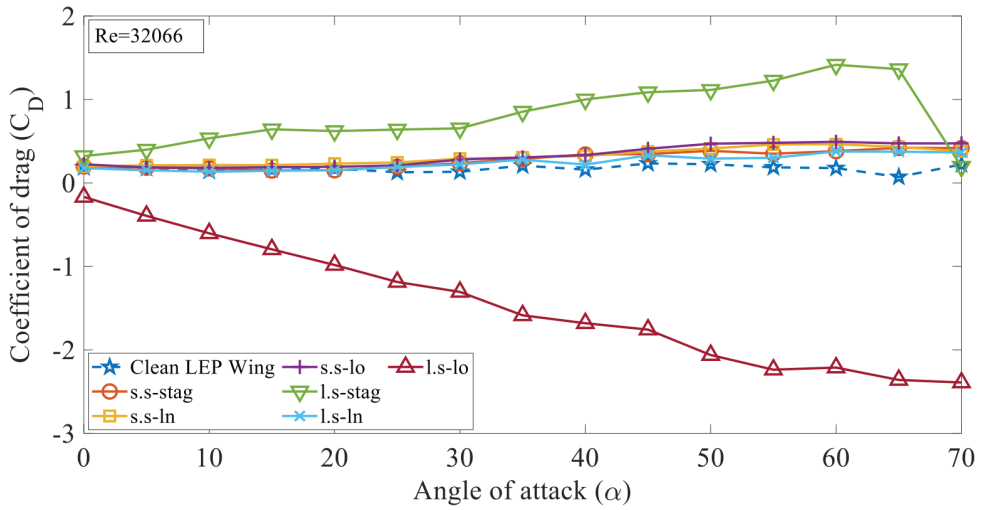

Figure 11. Coefficient of drag (CD) vs Angle of attack (α).

in the boundary layer by large shark scale with staggered non-overlapped alignment pattern might be a possible explanation for the unusual increment in the drag coefficient. Despite the increased drag, lift by drag ratio or aerodynamic efficiency is high and hence, aerodynamic performance is not compromised for the same. The baseline LEP wing has a very much lower drag when compared to the shark scale models at post-stall angles. However, at the pre-stall angles, it can be inferred from the Fig. 11 that the large shark scale models arranged in linear non-overlapped alignment pattern exhibits the lowest drag. Figure 12 demonstrates the comparison of lift coefficient over baseline and shark scale models. From Fig. 12 it is observed as the small shark scale structure reduces the flow acceleration over the airfoil in the pre-stall angles, it causes a reduction in the overall net pressure difference between the suction and the pressure side of the model thus resulting in lesser lift coefficient. However, at the same time, during post-stall angles, the same small shark scale structure enhances the turbulent mixing of the separated shear layers thus rendering the shark scale model advantageous. It can be easily seen from the Fig. 12 that beyond α=20°, LEP model with small shark scale structures exhibit higher lift coefficient in comparison against the baseline LEP model without shark scale structures. Evidently, large shark scale structures arranged in the staggered non-overlapped pattern exhibits a higher lift in comparison with other models even at greater angles of attack. The negative lift coefficient produced by model incorporating large shark scale structures arranged in linearly overlapped configuration can be seen clearly from the Fig. 12(a). This confirms the poor aerodynamic behaviour of the large shark scale structures arranged in linearly overlapped configuration as stated earlier. Figure 13 represents the comparison of drag coefficient over the baseline and shark scale models. Apparently, a higher-pressure drag is produced by the large shark scale structures arranged in the staggered non-overlapped pattern than other models which might be caused due to perturbation over the airfoil model. It can be concluded from the observations that the turbulence mixing induced by the shark scale structures creates perturbation over the airfoil thus increasing the pressure drag resulting in a higher drag coefficient than its counterpart unmodified equivalent. Experimental results revealed that each shark scale size and pattern have its own unique effects on aerodynamics of the airfoil in terms of maximum lift coefficient, minimum drag coefficient, stall delay characteristics etc. Hence, understanding the fundamental flow physics is therefore seen to be essential.

b) Re=69488:

The time-averaged lift coefficient as a function of angle of attack (α) for small and large shark scale geometries aligned in three different patterns are shown in Fig. 14. It is evident from the graphs that there is significant difference in the coefficient of lift between the three patterns model of both small and large shark scale structures and baseline LEP wing. This clearly shows that with the change in the alignment pattern, the surface flow shifts appreciably over the modified LEP airfoil. It can be inferred from the figure that the (C_L) of baseline LEP wing increases from α = 0° to 45° with a maximum C_L of 0.8650 at α=45°. Beyond which with the further increase in the angle of attack, stall phenomenon is initiated.

Aiming at identifying the aerodynamic lift for the modified models, initially, it was observed that the trendline of small shark scale structure aligned in staggered non-overlapped pattern, the C_L for 3D printed shark scale model increases as α increases to 40°, with $(C_L)_{max}$ = 0.8541. However, the lift coefficient for the same at pre-stall angles, say 15°, is 33.2% higher than its unmodified counterpart. Secondly, the C_L for small scale structure arranged in

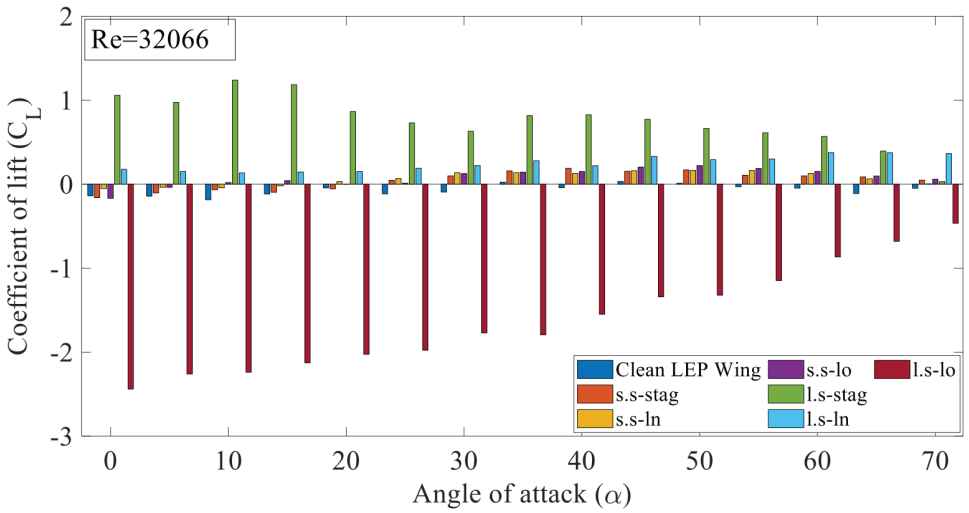

(a)

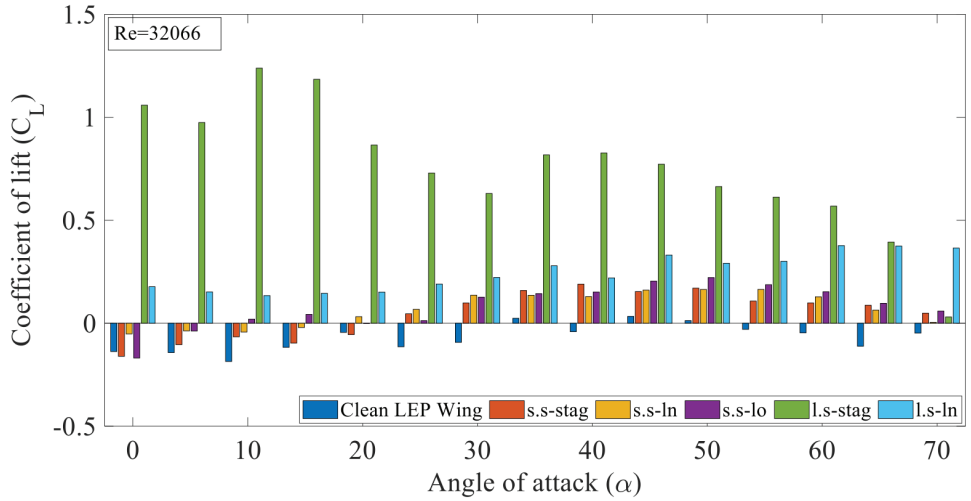

(b)

Figure 12. (a) Comparison of the coefficient of lift (C_L) over baseline and shark scale models (b) Comparison of the coefficient of lift (C_L) over baseline and shark scale models (better resolution)

linear non-overlapped structure exhibited a maximum C_L of 0.8823 which stalls at 50° offering significant stall delay. Subsequently, the lift coefficient for small scale structure arranged in linear overlapped structure increases till α = 20° and exhibits a small dip in the lift coefficient. It regains lift with a maximum lift coefficient of 0.8567 at α = 45°. Upon examining the lift coefficient curve for large shark scale structure aligned in staggered non-overlapped pattern, the C_L increases till 45° angle of attack with a maximum lift coefficient of 0.9425. The lift coefficient for large shark scale structure aligned in staggered non-overlapped pattern at post-stall regime, say 55°, has improved by 23.8% when compared to baseline LEP wing. The C_L for large shark scale structure aligned in linear non-overlapped pattern, represents increment as a function of an angle of attack in the increasing direction of angles of attack from 0° < α < 40° with a maximum lift coefficient of 0.8598 at α = 40°. It is also observed that all the shark scale models produce negative lift at initial angles of attack. A possible explanation to this observation could be, at α = 0° the baseline LEP wing section itself have attached flow. Moreover, the incorporation of the shark scales over the LEP wing section could acts as an obstruction leading to accumulation of pressure over suction side and hence, negative lift. From the above observations, it can be reported that the staggered non-overlapped pattern for small shark scale structure exhibit an enhanced aerodynamic performance in terms of lift coefficient in the pre-stall regime while staggered non-overlapped pattern for small shark scale structure enhances the performance in post-stall regime. Therefore, based on the results, it can be claimed that whatsoever pattern and size of shark scale structures, incorporation of the same plays

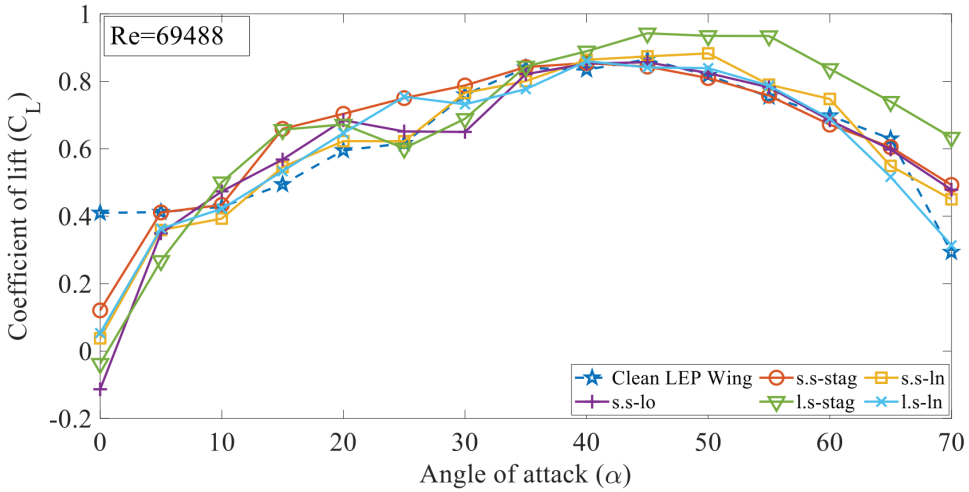

Figure 13. Coefficient of lift (C_L) vs Angle of attack (α).

a significant role in altering flow characteristics and renders better aerodynamic performance than its unmodified equivalent. Fig. 15 illustrates the variation of drag coefficient with angle of attack for all the test models. It can be noted from the figure that the C_D increases with the increase in angle of attack. Aiming at identifying the aerodynamic drag coefficient trendline for different arrangement of shark scale models, the drag coefficient for the large shark scale structures aligned in staggered non-overlapped pattern is lesser in the pre-stall angles than the baseline LEP wing. The modified airfoil with large shark scale structure staggered maintains a thinner, more energized boundary layer, keeping the flow attached over a greater portion of the surface. It is speculated that the staggered pattern infuses more momentum in to the flow thereby resulting in a smoother pressure distribution and reduced wake size, leading to a lower overall drag coefficient at pre-stalling angles. While, the C_D trendline for large shark scale structure arranged in linear non-overlapped pattern was similar to the trendline of baseline LEP wing. But, drag coefficient is lesser at pre-stalling angles in comparison with the baseline model. It can be inferred as the difference in the net pressure between leading-edge and trailing edge is less at pre-stall angles in the model integrated with shark scale structure arranged in linear non-overlapped configuration. The drag coefficient for small shark scale arranged in linear overlapped pattern is slightly higher when compared to baseline LEP wing. The higher drag might be associated with the trapping induced by the incidence angle of the overlapping shark scale structure which enhances the turbulence that eventually leads to increased drag. Overall, it is believed that the disturbance induced by the intensity of vortices generated from the

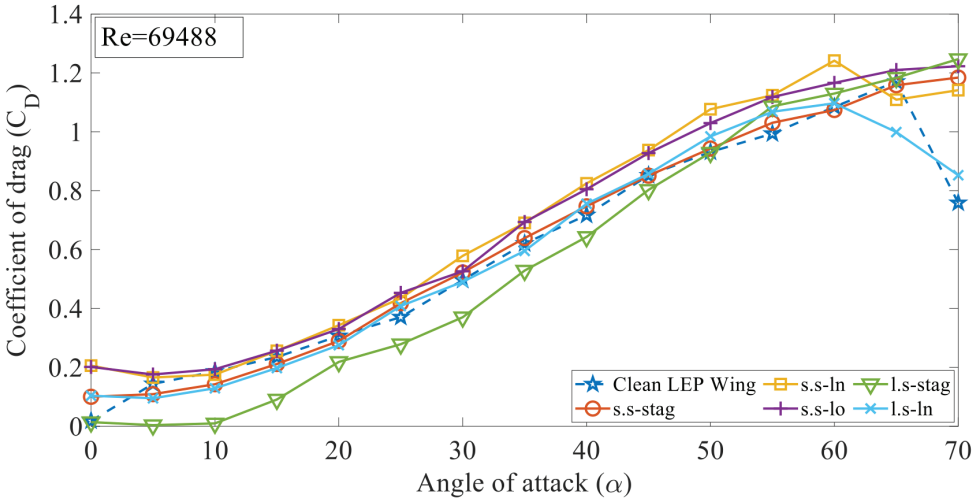

Figure 14. Coefficient of drag (C_D) vs Angle of attack (α).

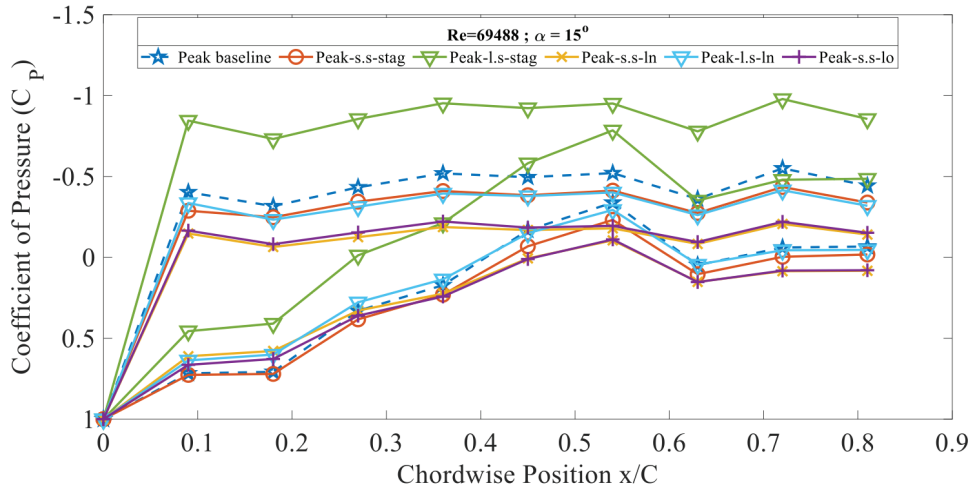

Figure 15. Pressure coefficient vs x/c at Re = 69488 at α = 15° (peak region).

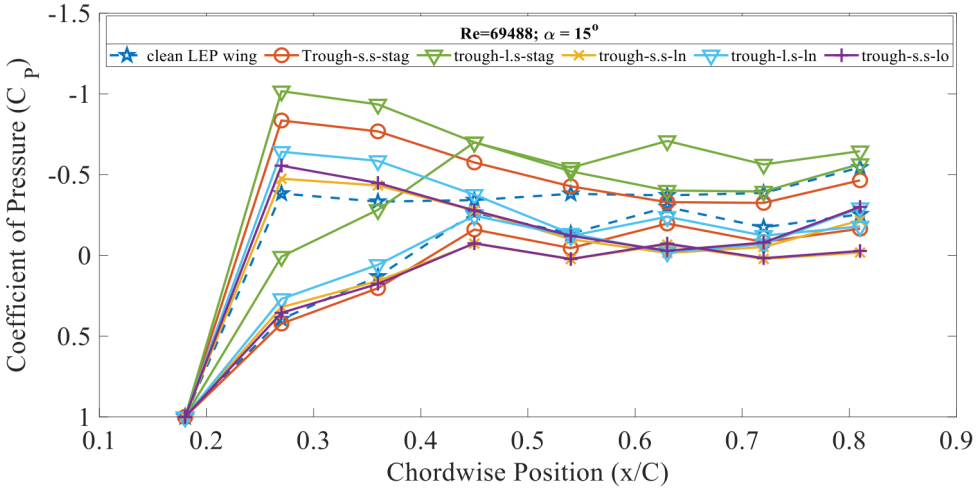

Figure 16. Pressure coefficient vs x/c at Re = 69488 at α = 15° (trough region).

shark scale structures might be the reason for the increase in overall drag coefficient.

Figure 16 & 17 depicts the coefficient of pressure (C_P) vs. chordwise position (x/C) for peak and trough section of all the test models at 15° angle of attack. It is evident that pressure distribution of the clean baseline LEP wing exhibits less negative pressure on the upper or suction surface of peak region till 40% of the chordwise location. This indicates the attached flow over the first 40% of the chordwise location and eventually the flow gets separated over the remaining chordwise location. On the other hand, the pressure distribution for other models except large shark scale aligned in staggered non-overlapped pattern exhibit a negative suction pressure in the vicinity of leading-edge which can be inferred from the Fig. 16. On investigating the large shark scale aligned in staggered non-overlapped pattern, the suction pressure decreases till 54% of the chordwise location indicating more attached flow over the peak section. Thus, it can be understood that the flow over the modified model incorporating large shark scales aligned in staggered non-overlapped pattern is accelerated effectively indicating delayed flow separation. It is worth noting that the pressure difference between the upper and lower surface of the modified test cases is higher than the baseline LEP wing representing higher lift coefficient. This can be confirmed from the Fig.14 and can be plausibly explained as the shark scales infuses energy into the boundary layer to the effectively accelerate flow at α = 15° in the peak section of the model. Further investigating the pressure distribution graph, it can be observed from the Fig. 16 that a low negative suction pressure is seen in the leading-edge region varying from -0.2 to -0.4 for all the models except for large shark scale

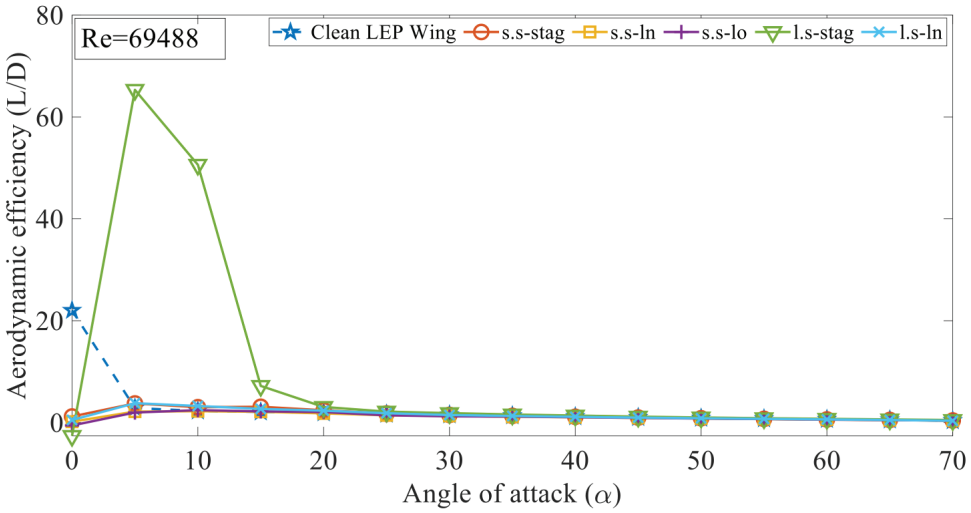

Figure 17. Aerodynamic efficiency (L/D) Vs angle of attack (α).

Table 5. Comparison of Results

Label	Parameter	Baseline	Modified	Benefits
s.s-stag	Lift Coefficient	0.49	0.66	34.6% increment in the C_L
l.s-stag	Drag Coefficient	0.31	0.22	29% decrement in the C_D
s.s-ln	Stall	35°	50°	Stall delay by 42.8%

model aligned in staggered non-overlapped pattern. In the case of large shark scale model arranged in staggered non-overlapped pattern, negative suction pressure is maximum than all the other test cases and present over the first 40%-50% of the chordwise location. It is observed that pressure varies linearly but fails to reach ambient pressure at the trailing edge vicinity. The pressure difference between the rear and front of the airfoil increases along the chordwise distance when flow over the airfoil separates, resulting in increasing in pressure drag. On examining Fig.17, it is identified that the pressure distribution in the trough section for the modified large shark scale model aligned in staggered non-overlapped pattern has a higher suction pressure which indicates the flow is accelerated over the trough section of the airfoil. From these observations, it becomes clear that the modified shark scale models effectively delay the flow separation in addition with increased lift.

Figure 17 represents the aerodynamic efficiency as a function of angle of attack. From the figure, it becomes clear that the efficiency of the modified model affixed with shark scale structure is relatively higher than the unmodified equivalent especially in the pre-stall regime. Though the modified models enhance the performance, linearly overlapped pattern of large shark scale structure outperforms the conventional LEP baseline model by injecting momentum from the free-stream into the boundary layer effectively which improves the aerodynamic efficiency. Moreover, the large shark-scale structure arranged in staggered non-overlapped pattern renders even more high performance than the linearly overlapped shark scale pattern. The linear overlapped pattern tends to behave like a riblet inducing momentum in to the flow along the line, whereas in the case of the staggered non-overlapped pattern, the vortices induced from the first line of shark scale gets more infusion of momentum due to the formation of the turbulent boundary layer. The small shark-scale structures also exhibit better performance than the baseline model. However, the amount of momentum induced by such small-scale structures are not sufficient enough to alter the flow characteristics favourably resulting in lesser performance characteristics than the large shark scale structures. Therefore, based on the results, it can be concluded that the staggered pattern of the large shark-scale structures offers more aerodynamic benefits and delay the flow separation more effectively. The summary of the comparison of results are tabulated in the Table 5.

CONCLUSION

A series of wind tunnel test were performed to investigate the effect of two different sized shark scale arranged in three different configurations over the test airfoil at multiple

Reynolds number. Based on the experimental evaluation the following conclusions were made as follows:

- Knowledge on the effect of shark scale flow control structures over the aerodynamic characteristics of a biologically inspired leading-edge protuberanced test model were highlighted and presented.
- Modified airfoil models fitted with shark scale structures performs significantly better than its unmodified equivalent by suitably altering the flow behavior over the airfoil.
- In terms of lift coefficient at pre-stall angles, the modified airfoil model exhibits better performance characteristics. Out of different shark scale patterns and two different Reynolds number tested it has been identified that the staggered non-overlapped pattern exhibits a peak lift increment of about 33.2% at $\alpha = 15^{o}$, when compared against the baseline Leading-Edge Protuberanced model.
- At post-stall angles, the shark scale structures featuring staggered non-overlapped pattern exhibits an enhanced aerodynamic lift performance with the maximum increment of 23.8% than the baseline model.
- At low Reynolds number conditions, the modified airfoil models outperform the conventional Leading-Edge Protuberanced model, making it as a better choice for applications, such as micro- and nano-aerial vehicles, shark scales are preferred.
- Incorporation of linearly non-overlapped pattern of small shark scale structured airfoil eliminates the two step stall characteristics behaviour present in the conventional Leading-Edge Protuberanced models and offers the aerodynamic benefit in terms of stall delay by stalling at $\alpha=50^{o}$.
- If drag reduction is of primary concern, then large-scale staggered shark scale structured airfoil can be employed for a peak drag reduction of about 28.7% in pre-stall angles at $\alpha=20^{o}$.
- Results reveal that the baseline Leading-Edge Protuberanced airfoils performs apparently poorer at the low-Reynolds number tested in this experiment. Moreover, with the addition of the shark scale structures it renders the aerodynamic benefit. Comparing the overall results, it has been observed that the large-scale staggered shark scale structure exhibits a peak 65.31% of aerodynamic efficiency increment than the baseline Leading-Edge Protuberanced model.

The experimental results proved that different pattern and sizes have unique features in altering the aerodynamics of flow. Since, the modified shark scale model is effective at low Reynolds number and at low angle of attack, it can be applied to Lighter Than Air technologies like airships where drastic change in angles of attack will not be very frequently utilized, Micro-Aerial Vehicles and Nano-Aerial Vehicles which fly at low Reynolds numbers. Since the 3D Printed shark scale geometries were pasted on the Leading-Edge Protuberanced wing section, the wind tunnel testing at high Reynolds number were carefully ignored to avoid dislodging of such 3D Printed structures which could be resolved in the future study with some other means. It is worth noting that the shark scale structures can be 3D printed directly on the wing model itself to avoid dislodging at higher Reynolds numbers, but at the price of more cost per model. Bristling angle and different patterns and sizes at higher Reynolds number testing along with the attempts to decode the underlying flow physics will be made in the near future to potentially utilize this technology in real-time.

NOMENCLATURE

LEP	Leading-edge protuberance
GAMBIT	Geometry And Meshing Built-In Tool
MAV	Micro-Aerial Vehicle
NAV	Nano-Aerial Vehicle
UAV	Unmanned-Aerial Vehicle
VG	Vortex Generator
SSVG	Shark Scale Vortex Generator
SEM	Scanning Electron Microscopy
λ	Wavelength
A	Amplitude
C	Chord length
PLA	Polylactic acid
F_D	Drag force
F_L	Lift force
ΔP	Net Pressure
S+	Effective Re based on shark scale spacing
S_i	Area
α	Angle of attack
θ	Angle of incidence on the i^{th} port
C_D	Coefficient of drag
C_L	Coefficient of lift
C_P	Coefficient of pressure
X/C	Chordwise location
Re	Reynolds Number
s.s-stag	Small shark scale - staggered non-overlapped pattern
s.s-ln	Small shark scale - linear non-overlapped pattern
s.s-lo	Small shark scale - linearly overlapped pattern
l.s-stag	Large shark scale - staggered non-overlapped pattern
l.s-ln	Large shark scale - linear non-overlapped pattern
l.s-lo	Large shark scale - linearly overlapped pattern

AKNOWLEDGEMENTS

The authors would like to thank SASTRA University for allowing us to carry out the wind tunnel experiments.

DATA AVAILABILITY STATEMENT

The authors confirm that the data that supports the findings of this study are available within the article. Raw data that support the finding of this study are available from the corresponding author, upon reasonable request.

CONFLICT OF INTEREST

The author declared no potential conflicts of interest with respect to the research, authorship, and/or publication of this article.

ETHICS

There are no ethical issues with the publication of this manuscript.

STATEMENT ON THE USE OF ARTIFICIAL INTELLIGENCE

Artificial intelligence was not used in the preparation of the article.

REFERENCES

[1] Choi H, Park H, Sagong W, Lee SI. Biomimetic flow control based on morphological features of living creatures. Phys Fluids 2012;24:121302. [CrossRef]

[2] Arunvinthan S, Raatan VS, Nadaraja Pillai S, Pasha AA, Rahman MM, Juhany KA. Aerodynamic characteristics of shark scale-based vortex generators upon symmetrical airfoil. Energies 2021;14:1808. [CrossRef]

[3] Hussein E, Azziz H, Rashid F. Aerodynamic study of slotted flap for NACA 24012 airfoil by dynamic mesh techniques and visualization flow. J Therm Eng 2021;7:230–9. [CrossRef]

[4] Mahmoud H. Stability of turbine blades, aircraft wings and their acoustic radiation. J Therm Eng 2015;1:6. [CrossRef]

[5] Ayli E, Koçak E, Türkoğlu H. Numerical investigation of rod–airfoil configuration aeroacoustic characteristics using Ffowcs-Williams-Hawkings equations. J Therm Eng 2021;7:58–70. [CrossRef]

[6] Alpman E. Aerodynamic performance of small-scale horizontal axis wind turbines under two different extreme wind conditions. J Therm Eng 2015;1:420–32. [CrossRef]

[7] Maheri A. Simulation of wind turbines utilising smart blades. J Therm Eng 2016;2:557–65. [CrossRef]

[8] Boumehani A, Noura B, Kerfah R, Khelladi S, Dobrev I. Numerical investigation of the blade profile effect on the aerodynamic performance of a vertical-axis wind turbine Darrieus H-rotor. J Therm Eng 2020;6:388–402. [CrossRef]

[9] Şumnu A, Güzelbey İ. The effects of different wing configurations on missile aerodynamics. J Therm Eng 2023;9:1260–71. [CrossRef]

[10] Tasif TH, Rahman MH, Fazle AB, Karim MM. Numerical prediction of flow past a marine rudder. Procedia Eng 2017;194:59–66. [CrossRef]

[11] Zanotti A, Menini L, Savino A, Grassi D, Riccobene L. Experimental investigation of wing-propeller aerodynamic interaction in eVTOL configurations. Aerosp Sci Technol 2024;152:109348. [CrossRef]

[12] Lang A, Hidalgo P. Cavity flow characterization of the bristled shark skin microgeometry. In: 47th AIAA Aerospace Sciences Meeting including the New Horizons Forum and Aerospace Exposition. 2009;1107. [CrossRef]

[13] Bechert DW, Bruse M, Hage W. Experiments with three-dimensional riblets as an idealized model of shark skin. Exp Fluids 2000;28:403–12. [CrossRef]

[14] Motta P, Habegger ML, Lang A, Hueter R, Davis J. Scale morphology and flexibility in the shortfin mako Isurus oxyrinchus and the blacktip shark Carcharhinus limbatus. J Morphol 2012;273:1096–110. [CrossRef]

[15] Wen L, Weaver JC, Thornycroft PJ, Lauder GV. Hydrodynamic function of biomimetic shark skin: Effect of denticle pattern and spacing. Bioinspir Biomim 2015;10:066010. [CrossRef]

[16] Wen L, Weaver JC, Lauder GV. Biomimetic shark skin: Design, fabrication and hydrodynamic function. J Exp Biol 2014;217:1656–66. [CrossRef]

[17] Yasuda Y, Zhang K, Sasaki O, Tomita M, Rival D, Galipon J. Manufacturing of biomimetic silicone rubber films for experimental fluid mechanics: 3D printed shark skin molds. J Electrochem Soc 2019;166:B3302–8. [CrossRef]

[18] Chien HW, Chen XY, Tsai WP, Lee M. Inhibition of biofilm formation by rough shark skin-patterned surfaces. Colloids Surf B Biointerfaces 2020;186:110738. [CrossRef]

[19] Domel AG, Saadat M, Weaver JC, Haj-Hariri H, Bertoldi K, Lauder GV. Shark skin-inspired designs that improve aerodynamic performance. J R Soc Interface 2018;15:20170828. [CrossRef]

[20] Lee C, Lee GW, Choi W, Yoo CH, Chun B, Lee JS, et al. Pattern flow dynamics over rectangular Sharklet patterned membrane surfaces. Appl Surf Sci 2020;514:145961. [CrossRef]

[21] Mawignon FJ, Liu J, Qin L, Kouediatouka AN, Ma Z, Lv B, et al. The optimization of biomimetic shark-skin riblet for the adaptation of drag reduction. Ocean Eng 2023;275:114135. [CrossRef]

[22] Li S, Liu S, Zhao D, Dong L, Jiao H. Drag reduction characteristics of the placoid scale array skin supported by micro Stewart mechanism based on penalty immersed boundary method. Appl Ocean Res 2024;149:104049. [CrossRef]

[23] Chen D, Cui X, Liu X, Chen H. Bionic gradient flexible fish skin acts as a passive dynamic micro-roughness to drag reduction. Surf Coat Technol 2023;457:129337. [CrossRef]

[24] Chen D, Liu X, Cui X, Zhang L, Chen H. Research progress and development trend of the drag reduction inspired by fish skin. Prog Org Coatings 2023;182:107613. [CrossRef]

[25] Chen D, Li W, Zhao Y, Liu J, Cui X, Zhao Z, et al. Drag reduction capacity of multi-scale and

multi-level riblet in turbulent flow. Biosurf Biotribol 2024;10:7−15. [CrossRef]
[26] Arunvinthan S, Pillai SN, Cao S. Aerodynamic characteristics of variously modified leading-edge protuberanced (LEP) wind turbine blades under various turbulent intensities. J Wind Eng Ind Aerodyn 2020;202:104188. [CrossRef]
[27] Bar-Cohen Y. Biomimetics: Biologically inspired technologies. Boca Raton (FL): CRC Press; 2005. [CrossRef]
[28] Anderson JD Jr. Fundamentals of aerodynamics. New York: McGraw-Hill; 2016.
[29] Li QA, Kamada Y, Maeda T, Murata J, Nishida Y. Effect of turbulent inflows on airfoil performance for a horizontal axis wind turbine at low Reynolds numbers (Part I: Static pressure measurement). Energy 2016;111:701−12. [CrossRef]
[30] Arunvinthan S, Pillai SN. Aerodynamic characteristics of unsymmetrical aerofoil at various turbulence intensities. Chin J Aeronaut 2019;32:2395−407. [CrossRef]
[31] Arunvinthan S, Gouri P, Divysha S, Devadharshini RK, Nithya Sree R. Effect of trough incidence angle on the aerodynamic characteristics of a biomimetic leading-edge protuberanced (LEP) wing at various turbulence intensities. Biomimetics 2024;9:354. [CrossRef]
[32] Barlow JB, Rae WH, Pope A. Low-speed wind tunnel testing. New York: John Wiley & Sons; 1999.

APPENDIX

The shark scales and baseline models were 3D printed using Neptune 4 Plus FDM 3D printer with the tolerance of ±0.1 mm. The primary design of base model and shark scale models were made using gambit which was exported as .iges file. The same has been converted to .stl file and analysed the models in Klipper software which was provided along with the OEM of 3D printer to test for the wall thickness parameter and location of pressure taps etc. The feasibility check was then run through the klipper software. Following which, the models were then 3D printed using Neptune 4 Plus FDM 3D printer using PLA Material. The 3D printed models were then post-processed using a series of abrasive sheets to obtain ultra-marble finish. Later, the specimens were blown with a compressed air to remove any mechanical burrs etc before testing.

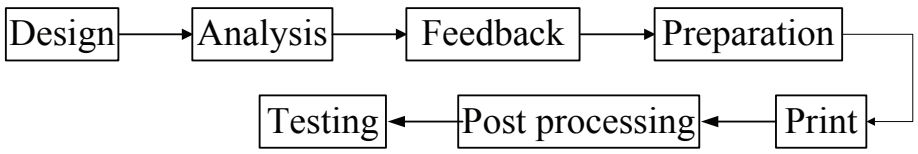

Basic flow chart depicting the 3D printing process